RSC Advances

PAPER

View Article Online
View Journal | View Issue



Cite this: *RSC Adv.*, 2023, **13**, 239

# Amphiphilic di-cationic methylene blue for improving antibacterial photodynamic efficiency through high accumulation and low aggregation on bacterial cell surfaces

Hao Zhang,†[a] Lixian Xu,†[b] Xiaoxiao Gu,[a] Dinghua Yu *[a] and Shuang Li[a]

The aggregation state of photosensitizers on the surface of bacterial cells is an important scientific problem for antibacterial photodynamic therapy (APDT). High accumulation and high photoactive state maintenance of photosensitizers are the prerequisite of high APDT efficiency. In this study, an amphiphilic di-cationic methylene blue photosensitizer ($C_{12}$-MB) was synthesized through quaternization, and its structure, interface properties, photophysical properties and antibacterial photodynamic properties were studied. The results showed that $C_{12}$-MB could reduce 4.27 $\log_{10}$ CFU and 4.8 $\log_{10}$ CFU for *P. aeruginosa* and *S. aureus* under irradiation of light at 660 nm, higher than the parent methylene blue. Through a spectroscopic study on photosensitizer adsorption over the bacterial surface, $C_{12}$-MB can be accumulated with higher concentration, and the photo-active monomer content is 73% and 70% over *P. aeruginosa* and *S. aureus*, higher than those of methylene blue: 25% and 49%, respectively. The higher content of non-aggregated photo-active monomer could contribute to higher antibacterial photodynamic efficiency. For $C_{12}$-MB adsorbed over bacterial surfaces, planar packing inhibition and electrostatic repulsion could contribute to lower $C_{12}$-MB aggregation, which provides an useful reference for the structural design of high-efficiency photosensitizers.

Received 14th October 2022
Accepted 15th December 2022

DOI: 10.1039/d2ra06484g

rsc.li/rsc-advances



## 1 Introduction

COVID-19 once again showed the struggle between human beings and microbes, and the war with pathogenic microorganisms will continue forever. After penicillin was firstly discovered by British bacteriologist Alexander Fleming in 1928, antibiotics were one of the most significant medical achievements of the 20th century.[1] With the continuous research and development of new antibiotics, human beings defeated pathogenic microorganisms. However, due to the abuse of antibiotics, drug-resistant bacteria have emerged one after another. Multi-drug resistance has induced many infectious illnesses, which has seriously threatened human health in the "post-antibiotic" era as stated by the WHO.[2] Due to its multi-target action modes, antimicrobial photodynamic therapy (APDT) has been reported in response to the severe challenges of the ever-growing antibiotic resistance.[3] Photodynamic therapy, due to the highly cytotoxic singlet oxygen or radical oxygen species (ROS) from photochemical reaction of oxygen and photosensitizers under light illumination, has found broad application in clinical fields such as hematology, dermatology, oncology, stomatology, cardiovascular, ophthalmic and infection science.[4–8]

The development of new photosensitizers and novel delivery systems is a permanent research subject of photodynamic therapy. Many previous research studies have revealed that the quantum yield of singlet oxygen depends heavily on the aggregation state of photosensitizers, which directly determined photodynamic therapy efficiency. For example, due to extreme hydrophobicity of the aromatic macrocycle and planarity, phthalocyanine photosensitizer has low solubility and serious aggregation in polar environment, which has weakened seriously its photodynamic efficiency.[9] Similar to hydrophobic photosensitizers, hydrophilic methylene blue could also aggregate in aqueous solution.[10] In order to inhibit photosensitizers aggregation, many novel delivery systems, such as liposomes,[11,12] surfactants vesicles[13] and microencapsulation,[14] have been developed.

On the other hand, the selective accumulation of photosensitizers on the target cells is another important factor to determine the efficiency of antibacterial photodynamic therapy. Comparing with nonionic and anionic photosensitizers, cationic photosensitizers could accumulate more over negatively-charged bacterial cells surfaces through electrostatic

[a]*College of Biotechnology and Pharmaceutical Engineering, Nanjing Tech University, Nanjing 211816, P. R. China. E-mail: yudh@njtech.edu.cn; Tel: +86-25-58139386*
[b]*Department of Dermatology, The Second Affiliated Hospital of Nanjing Medical University, No. 121 Jiangjiayuan Road, Nanjing 210000, P. R. China*
† These authors contribute equally to this paper and should be considered as co-first author.

interaction. With high quantum yield of singlet oxygen, cationic methylene blue has been used as an effective candidate for APDT due to high bioaccumulation over pathogenic microorganisms.[15] Durantini *et al.* has developed tricationic Zn(II) phthalocyanine derivative photosensitizers, and the multicationic photosensitizers could rapidly bind to microbial cells, and inactivate *S. aureus*, *E. coli* and *C. albicans* under light illumination.[16] Conti *et al.* reported that the structural characteristics of polyamine ligands gathered on highly charged Ru(II)-polypyridyl complexes could achieve a notable phototoxicity for *B. subtilis*.[17] Vitor *et al.* reported that photosensitizers in sodium dodecyl sulfate (SDS) solution reduced more bacteria compared to blank in that SDS could decrease the interfacial tension between the photosensitizer and the microorganisms and increase their transmembrane permeability.[18] Moreover, compared to anionic surfactant, cationic surfactants showed better antibacterial activity.[19] These research results provide a valuable references for the photosensitizers development of low aggregation and high accumulation. However, most of these studies focus on the aggregation states of photosensitizer in aqueous solution. When the photosensitizer is adsorbed on the target cells surfaces, it is inevitable to show a concentration increase, which is prone to aggregate and then reduces APDT efficiency. Therefore, designing photosensitizers that can maintain low aggregation on the pathogens surface will be an important goal of photodynamic drug development.

Here, amphiphilic di-cationic methylene blue derivative ($C_{12}$-MB) has been synthesized through quaternization of methylene blue and 1-bromododecane. The interfacial and photophysical properties results showed that the as-synthesized $C_{12}$-MB showed amphiphilicity and singlet oxygen production capability under 660 nm light illumination. The *in vitro* antibacterial photodynamic therapy showed that $C_{12}$-MB could reduce 4.27 $\log_{10}$ CFU and 4.8 $\log_{10}$ CFU for *P. aeruginosa* and *S. aureus*, higher than parent methylene blue, respectively. The photosensitizers states over bacterial cells surface disclosed by spectroscopic methods showed that the synthesized $C_{12}$-MB photosensitizer could be tightly accumulated with high concentration, and could maintain the monomer state of high photodynamic activity. These unique characteristics finally produced excellent antibacterial photodynamic efficiency.

# 2 Materials and methods

## 2.1 Materials

Methylene blue (MB), 1-bromododecane, pyrene, methyl orange (MO), dodecyl trimethyl ammonium bromide (DTAB) and 9,10-diphenylanthracene (DPA) were purchased from Aladdin Regent Co., Ltd (Shanghai, China). In addition, LB broth powder and LB agar powder were purchased from Sangon Biotech (Shanghai, China). All other reagent were purchased from Aladdin Regent Co., Ltd (Shanghai, China) without further purification.

*P. aeruginosa* YM4 (CCTCC No. M2017494) was provided by Prof. Shuang Li, Nanjing Tech University. *S. aureus* (CICC No. 21600) were kindly supplied by Dr Lixian Xu, the second affiliated hospital of Nanjing Medical University.

## 2.2 Methods

**2.2.1 Synthesis and characterization of $C_{12}$-MB.** Briefly, ethanol solutions of MB (30 mL, 3 mM) and 1-bromododecane (0.96 ml, 4 mmol) were mixed and sonicated for 30 min. The mixture was transferred into a Teflon-lined autoclave and sealed before being hydrothermally heated in an oven at 150 °C for 12 h. After cooling, the crude product was recovered through precipitation with diethyl ether (v/v = 1 : 5). After the solvent was removed by centrifugation, the black powder was dried under vacuum at 60 °C for 24 h. Finally, the solid was collected and labeled as $C_{12}$-MB (1.59 mg, yield: 85.41%, purity: 92.3%). The structure was characterized by $^1$H NMR (Brucker spectrometer, 400 MHz) and $^{13}$C NMR (Brucker spectrometer, 101 MHz) analyses, and the solvent was deuterium oxide and DMSO-d6, respectively.

High resolution electrospray ionization mass spectra (HR-ESI-MS) were obtained on Shimadzu LCMS-IT-TOF system. The positive ion mode was used in the ESI mass spectrometer with detector voltage of 1.57 kV and the temperature of curved desolvation line was set as 200 °C. The nebulizing gas flow rate was 1.5 L min$^{-1}$, and the drying gas pressure was set as 110.0 kPa.

$^1$H NMR (400 MHz, deuterium oxide) $\delta$ 7.05 (d, $J$ = 9.2 Hz, 3H), 6.68 (d, $J$ = 8.4 Hz, 2H), 3.06 (dd, $J$ = 13.2, 8.0 Hz, 6H), 1.17–1.01 (m, 22H), 0.99 (d, $J$ = 7.3 Hz, 6H), 0.97–0.93 (m, 3H).

$^{13}$C NMR (101 MHz, DMSO-d6) $\delta$ 135.29, 122.18, 115.35, 72.52, 54.10, 49.21, 31.74, 27.28, 10.51.

ESI-MS [$m/z$]: 298.136 $(M - C_{10}H_{23})^+$, 312.1509$(M - C_9H_{21})^+$.

Cationic characteristics of $C_{12}$-MB photosensitizer was tested by classic color reaction of potassium ferricyanide. The solution of $C_{12}$-MB and $K_3[Fe(CN)_6]$ were mixed and stirred.

**2.2.2 Surface tension.** The solutions of $C_{12}$-MB with different concentration were prepared by dissolving $C_{12}$-MB in the mixed solvent of deionized water and DMSO (v/v = 9 : 1) because of the poor water solubility. The surface tension was measured by the platinum ring detachment method (du Nouy's method) on the automatic tensiometer (BZY-3B, Shanghai Hengping instruments Co). The deionized water (72 mN m$^{-1}$) was used as standard solution at room temperature. The minimum surface tension and critical micelle concentration (CMC) of $C_{12}$-MB could be calculated from the surface tension curves. Moreover, the surface tension of DTAB solution was also measured as a positive control to analyze the effect of hydrophilic head on the aggregation behaviors of the surfactant in water.

**2.2.3 Microenvironment characterization.** Methyl orange (MO) and pyrene are two kinds of probe molecules to explore the microenvironment change of surfactant assembly. The hydrophobicity of surfactant assembly was reflected by methyl orange method described before with minor modification.[20] The UV absorption spectra of MO mixed with MB and $C_{12}$-MB respectively were recorded in the range of 350–540 nm. The concentration of MO was always kept at 20 mM.

The fluorescence spectra of pyrene were measured as reported before.[21] The methanol solutions of pyrene (300 μL, 5 g L$^{-1}$) was prepared, and the solvent was evaporated by the oven

 

at 60 °C for 5 h. Then, the aqueous solutions of MB and $C_{12}$-MB were added to the tube with pyrene, and sonicated for 30 min. The fluorescence spectra were recorded from 350–420 nm. The excitation wavelength of pyrene was 335 nm, and the excitation and emission slits were 5 nm.

**2.2.4 Photophysical properties.** The UV absorption spectra were measured by UH3000 UV spectrophotometer (Hitachi, Japan) with quartz cells. The concentration of MB and $C_{12}$-MB was kept at 6.25 μM. Then, the UV absorption spectra were recorded in the wavelength range of 250–800 nm at a scanning rate of 400 nm $min^{-1}$. The fluorescence spectra of MB and $C_{12}$-MB were recorded using the fluorescence spectrophotometer (F-7000, Hitachi, Japan) equipped with quartz cell in the wavelength range of 650–800 nm. The excitation wavelength was 600 nm, and the excitation and emission slits were 10 nm. The concentration of MB and $C_{12}$-MB was kept at 25 μM.

**2.2.5 Quantum yields and kinetics of singlet oxygen ($^1O_2$).** According to the previous report,[22] DPA oxidation was used as the probe reaction to measure quantum yields and kinetics of singlet oxygen based on absorption reduction of DPA. Firstly, MB and $C_{12}$-MB (75 μL, 4 mM) were added to the acetonitrile solution of DPA (40 mL, 0.1 mM) with stirring for 5 min, respectively. Then, the mixture was illuminated by a 660 nm LED light source (Shenzhen Sanxin Optoelectronic Technology Co., Ltd) with 30 mW $cm^{-2}$ output power for the different radiation time, and the absorption intensity change of the reaction solution at 372 nm was used to calculate the quantum yields and kinetics of singlet oxygen.

**2.2.6 *In vitro* antibacterial photodynamic assay.** *P. aeruginosa* and *S. aureus* were cultured according to the previous report.[23] Both strains were inoculated in LB medium, which were cultured at 37 °C in 200 rpm for 12 h. The bacterial content of *P. aeruginosa* and *S. aureus* is about $10^8$ CFU $ml^{-1}$ and $10^{10}$ CFU $ml^{-1}$.

Bacteria cultures in PBS (50 mL) were incubated with 200 μM photosensitizer for 30 min in the dark at 37 °C with 200 rpm to promote the combination of photosensitizer and cells. Then, 200 μL of mixture was plated on LB agar medium. The agar plates were irradiated for 60 min with a 660 nm LED light source with 30 mW $cm^{-2}$ output power, and then cultured at 37 °C for 24 h to observe bacteria growth. The cell viability was determined by the CFU on the agar plate through the serial dilutions in PBS. The experiments were repeated for three times with two replicates.

**2.2.7 Photosensitizer accumulation assay.** The bacterial contents of *P. aeruginosa* and *S. aureus* were kept in $10^8$ CFU $ml^{-1}$ and photosensitizers were maintained at 400 mM. The bacterial suspensions were incubated with photosensitizers for 30 min at 25 °C away from light. Then, the bacterial suspensions were centrifuged at 8000 rpm for 10 min to collect bacterial cells. The bacterial cells were washed by PBS repeatedly, and the UV absorption spectra of supernate were recorded to explore the elution ratio of photosensitizers. The fluorescence images of bacterial cells washed were obtained from a fluorescence microscopy (Olympus CX43, Tokyo, Japan). The photosensitizers accumulation over bacteria was calculated by the fluorescence standard curve of photosensitizers. In detail, the bacteria cells washed were broken by ultrasonic cell grinder for 20 min. The fluorescence spectra of bacteria cells were measured by the fluorescence spectrophotometer.

**2.2.8 Photosensitizer aggregation assay.** The adsorption-induced aggregation of photosensitizers was analyzed through UV-Vis absorption protocol. The bacterial cells washed were dispersed into PBS solution, which were subjected to UV-Vis absorption and fluorescence emission tests. The absorption at 660 nm could be indexed to monomer MB or $C_{12}$-MB, and the absorption at 585–605 nm could be attributed to multi-mer (including dimer, trimer, tetramer or other higher aggregation) aggregation. The absorption peaks area ratio of monomer and multi-mer was used to calculate the photosensitizers aggregation percent.

**2.2.9 Scanning electron microscopy.** After the bacterial suspensions of *P. aeruginosa* and *S. aureus* were incubated with MB and $C_{12}$-MB for 30 min in the dark condition and irradiated for 60 min, the mixtures were freeze-dried and the acquired powder samples were subjected to record bacteria morphology by scanning electron microscopy (SEM) using a SEMFEI quanta 250.

# 3 Results and discussion

## 3.1 $C_{12}$-MB synthesis and structures

Amphiphilic di-cationic methylene blue derivatives have been synthesized through quaternization as illustrated in Fig. 1(A). Due to the lower reaction activity of 1-bromododecane, the quaternization couldn't proceed under atmospheric pressure and moderate temperature (<100 °C). Therefore, the quaternization of 1-bromododecane and methylene blue was performed through autoclave hydrothermal process at 150 °C for 12 h. The structure of $C_{12}$-MB was characterized by $^1$H NMR and $^{13}$C NMR spectroscopy, and the results were shown in Fig. 1(B) and (C). The chemical shifts at around 0.85 ppm and 1.23 ppm could be attributed to the hydrogen atoms in $-CH_3$ and $-CH_2$ groups of long chain aliphatic hydrocarbons. The chemical shifts at 6.72–7.94 ppm belongs to the hydrogen atoms of the benzene ring in phenothiazine.[24] From $^{13}$C NMR results shown in Fig. 1(C), the chemical shifts at 27.28 ppm symbolize the carbon atoms of long alkyl chain, and those around 115 ppm, 122 ppm and 135 ppm could be attributed to the carbon atoms on aromatic ring. The result of mass spectra has been showed in Fig. 1(D). Two intense product ion peaks at *m*/*z* 298.1360 ($C_{17}H_{20}N_3S$) and *m*/*z* 312.1509 ($C_{18}H_{22}N_3S$) were formed by fragmentation of long chain alkyl. MS fragmentation profiles showed peaks at *m*/*z* 298.1360 and *m*/*z* 312.1509 with the loss of $C_{11}H_{23}$ and $C_{10}H_{21}$, agreed with the results reported by Nichols.[25] The result of cationic characteristics experiment was shown in Fig. 1(E). The sediment was appeared in the mixture of $C_{12}$-MB and $K_3[Fe(CN)_6]$, which could be attributed to cationic of quaternary ammonium. According to Zhang's *et al.* research, quaternary ammonium functional group was applied for adsorption of metal cyanide.[26] These results demonstrated that the amphiphilic di-cationic photosensitizers $C_{12}$-MB have been synthesized successfully, which includes hydrophilic phenothiazine and hydrophobic hydrocarbon chain.

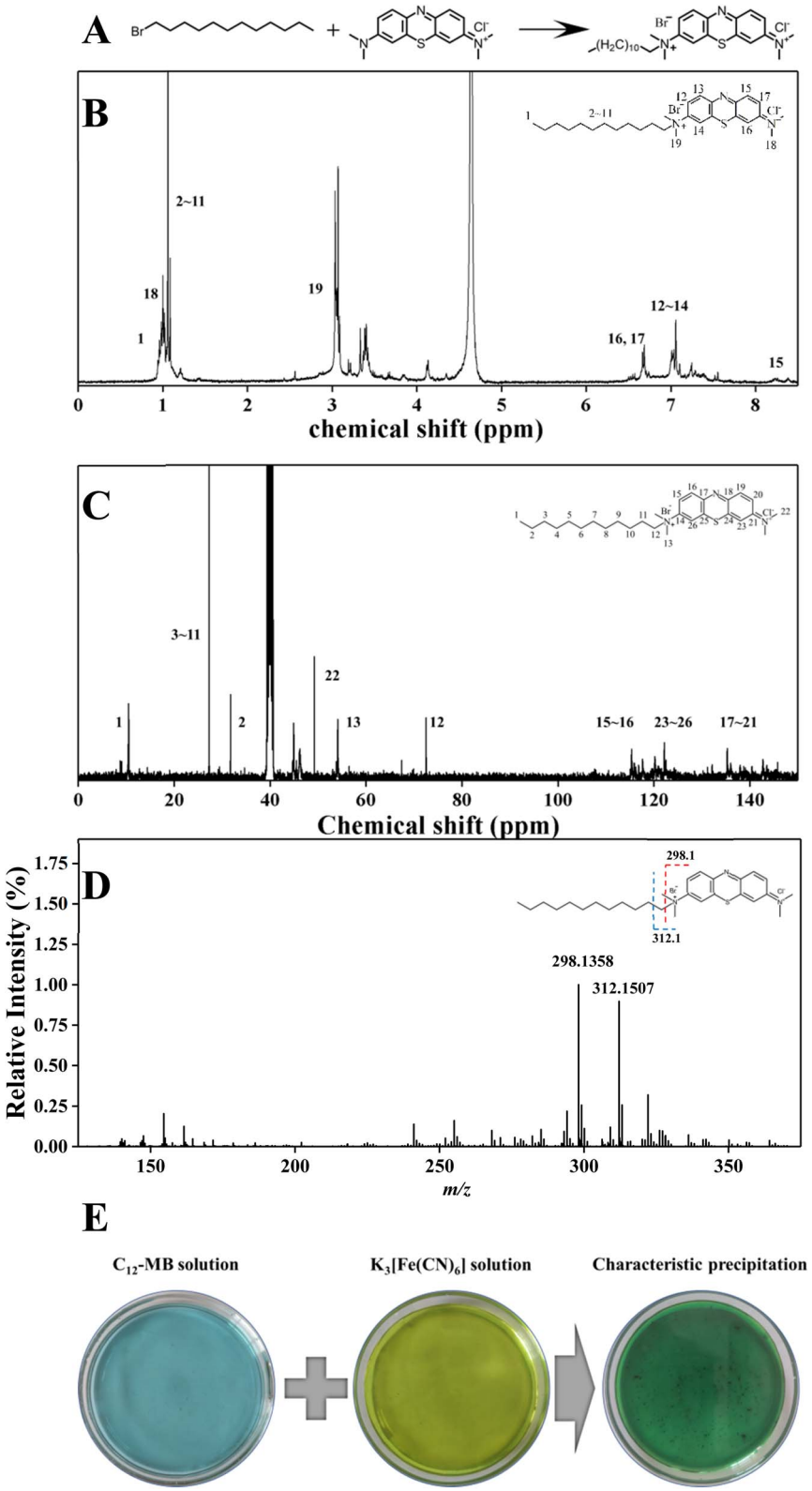


Fig. 1 The synthesis and structural characterization of amphiphilic $C_{12}$-MB photosensitizers. (A) The synthesis diagram. (B) $^{1}H$ NMR spectra. (C) $^{13}C$ NMR spectra. (D) High resolution electrospray ionization mass spectra. (E) Identification of positive charge of quaternary ammonium salt.

### 3.2 Surface and micelle properties

The surface tension of $C_{12}$-MB and DTAB solution with different concentration has been recorded as shown in Fig. 2(A) and (B) showed the corresponding fitted surface tension-ln($C$) results. From Fig. 2(B), the excess surface concentration ($\Gamma$) and the area occupied by the molecule to micelle ($A$) were calculated according to the classic model,[27] and the corresponding results have been listed in Table 1. Calculated from Fig. 2, the critical micelle concentration (CMC) of $C_{12}$-MB and DTAB is 1.623 $\times$ $10^{-3}$ mol $L^{-1}$ and 2.85 $\times$ $10^{-3}$ mol $L^{-1}$, respectively, and the minimum surface tension was 33.4 mN $m^{-1}$ and 22.6 mN $m^{-1}$, respectively. Comparing with DTAB, amphiphilic $C_{12}$-MB showed the lower CMC and higher minimum surface tension values, which could originate from structure differences. Possibly, the complicated hydrophilic phenothiazine structure of $C_{12}$-MB decreased its surface activity. According to Tomoharu's results, hydrophilic multi-ring structure could decrease the surface activity of amphiphilic molecules, which would result in higher surface tension and lower CMC.[28]

From Table 1, the $A$ value of $C_{12}$-MB and DTAB is 86.52 Å$^2$ and 116.98 Å$^2$, respectively. On the other hand, the $\Gamma$ value of $C_{12}$-MB and DTAB is 1.92 μmol $m^{-2}$ and 1.42 μmol $m^{-2}$. The results indicate that the occupied area of $C_{12}$-MB at the air–water interface is smaller than DTAB, and more $C_{12}$-MB molecules have been adsorbed at the air–water interface than DTAB. These surface properties differences could originate from the structure difference of $C_{12}$-MB and DTAB, furthermore, the hydrophilic head differences. Agreed with Miyake's results,[29] comparing with the quaternary ammonium salt structure, hydrophilic phenothiazine derivatives provide complex planar structure, which could form planar aggregation at air–water surface.

Table 1 Adsorption parameters of $C_{12}$-MB and DTAB at 298 K

| System | CMC ($10^{-3}$ M) | $\Gamma$ (μmol $m^{-2}$) | $A$ (Å$^2$) | Minimum surface tension (mN $m^{-1}$) |
|---|---|---|---|---|
| $C_{12}$-MB | 1.623 | 1.92 | 86.52 | 33.4 |
| DTAB | 2.850 | 1.42 | 116.98 | 22.6 |

Two kinds of dyes, methyl orange and pyrene, were used to probe the micelle microenvironment of $C_{12}$-MB and DTAB,

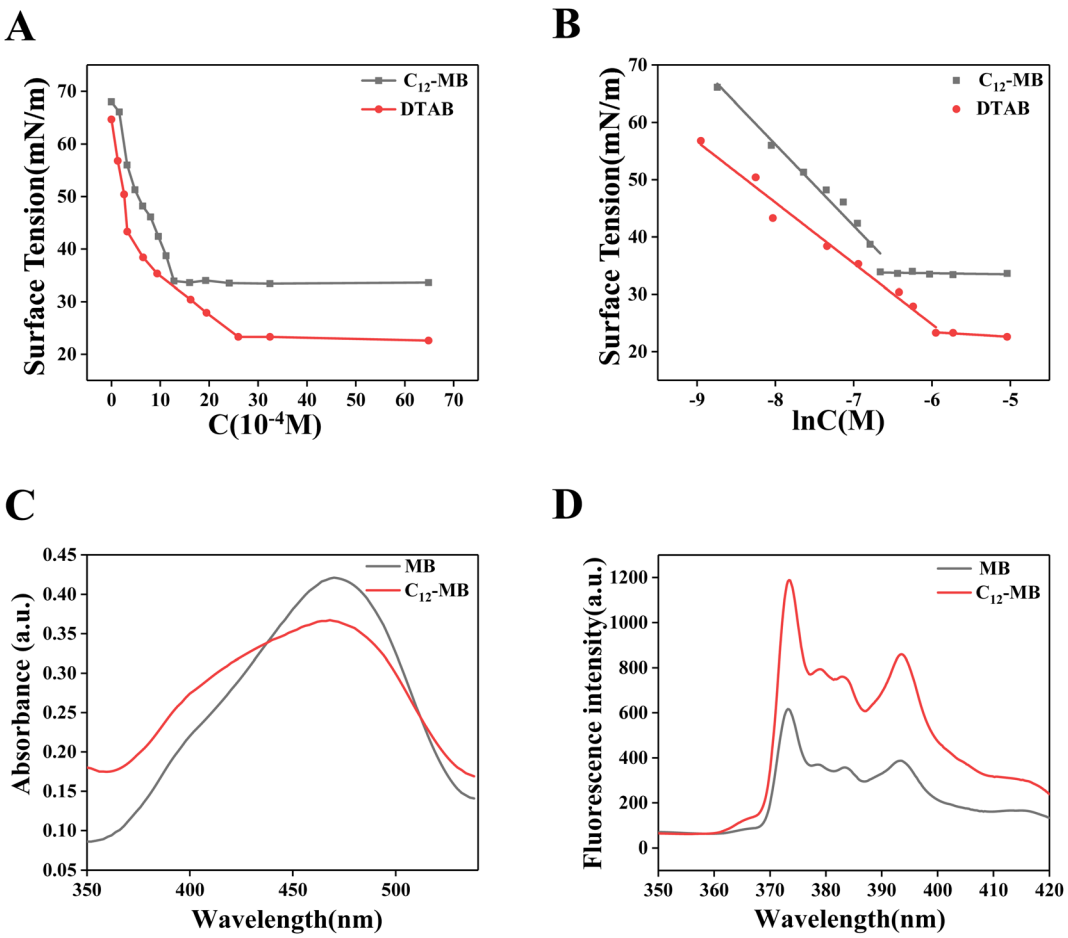


Fig. 2 The surface properties of $C_{12}$-MB and micelle microenvironment characterization by methyl orange and pyrene. (A) The surface tension curves of amphiphilic $C_{12}$-MB with DTAB as comparison. (B) The corresponding fitted surface tension-ln($C$) results of surface tension curves (C) Methyl orange absorption spectra in MB and $C_{12}$-MB solutions. Concentration: 20 mM (D) fluorescence spectra with pyrene as the fluorescent probe in MB and $C_{12}$-MB solutions. Concentration: 400 μmol $L^{-1}$.

and the corresponding UV-Vis absorption spectra and fluorescence emission spectra have been recorded and illustrated in Fig. 2(C) and (D). From Fig. 2(C), methyl orange in $C_{12}$-MB solution showed the higher absorption at 380 nm than that in MB solution. According to Karukstis's results, methyl orange in surfactant solution at concentrations below the CMC could show a new absorption peak at 374 nm except the peak at 470 nm, which could be attributed to hydrophobic microenvironment.[20] These results confirm the existence of hydrophobic microenvironment provided by amphiphilic $C_{12}$-MB assembly.

Pyrene is often used to disclose the microenvironment of surfactants solution.[21] The intensity ratio of the first and the third peaks ($I_1/I_3$) is sensitive to micropolarity. As shown in Fig. 2(D), fluorescence intensity of pyrene in $C_{12}$-MB solution was higher than that in MB solution. Furthermore, the $I_1/I_3$ values in solution of $C_{12}$-MB and MB are 1.56 and 1.72, respectively. The decreased $I_1/I_3$ value in $C_{12}$-MB solution indicated that $C_{12}$-MB could assemble and produce the hydrophobic microenviroment.

### 3.3 Photophysical properties

The photophysical properties of MB and $C_{12}$-MB have been characterized by UV-Vis absorption and fluorescence emission spectroscopy, and the corresponding results have been demonstrated in Fig. 3(A) and (B). As shown in Fig. 3(A), $C_{12}$-MB showed the similar absorption pattern to MB, including stronger absorption peaks at 664 nm and weaker peaks at 615 nm, which could be attributed to monomer and dimer aggregate forms, respectively.[30] Comparing with MB, $C_{12}$-MB showed the absorption peak red shift from 664.5 nm to 668.0 nm. On the other hand, $C_{12}$-MB showed weaker absorption than MB in the visible light region, which could be induced by $C_{12}$-MB micelle assembly. Cao *et al.* reported that dye in surfactant micelle showed decreased absorption properties.[31] On the other hand, both MB and $C_{12}$-MB showed the similar absorption at 293 nm, which indicated that long hydrocarbon chain was not grafted to the nitrogen atoms of phenothiazine. From fluorescence emission spectra in Fig. 3(D), the intrinsic fluorescence intensity of MB is stronger than that of $C_{12}$-MB, and the peak has blue-shifted to 694.0 nm compared with the peak at 691.6 nm of MB.

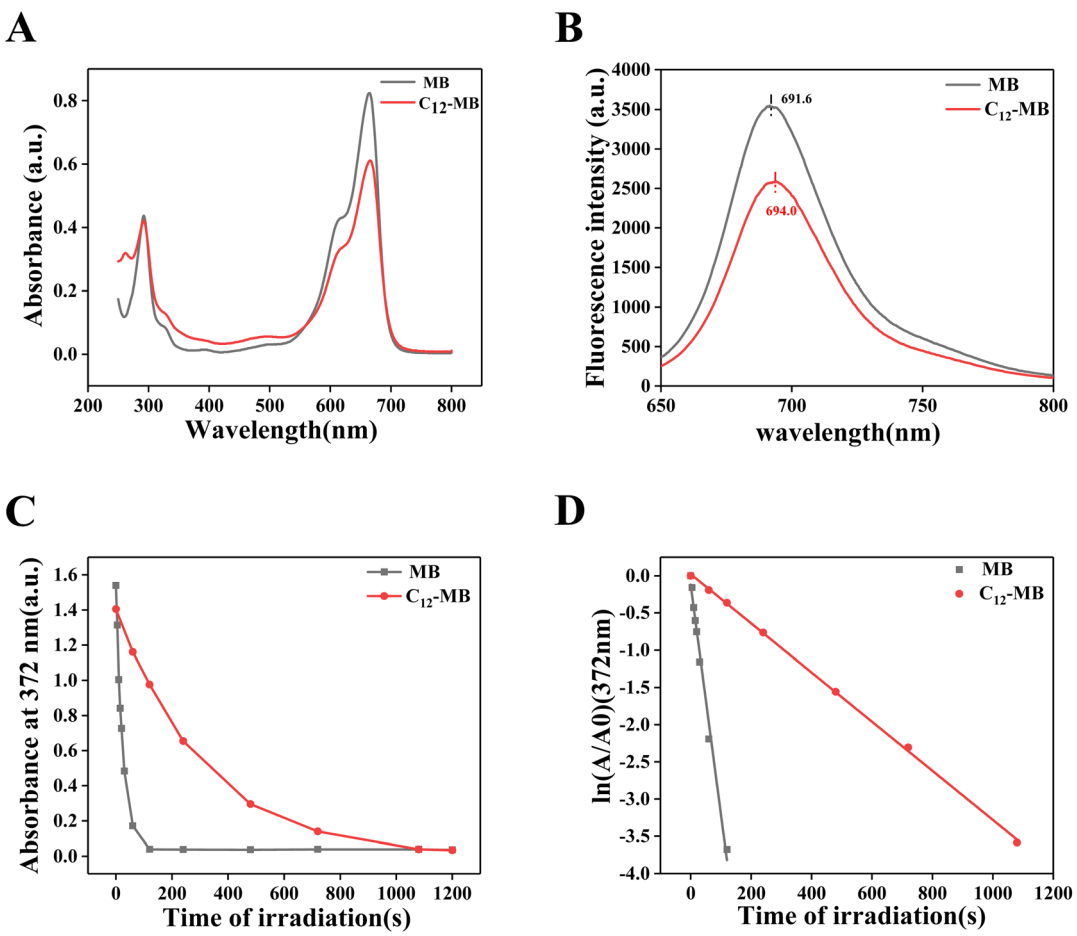


Fig. 3 The photophysical properties of methylene blue and $C_{12}$-MB. (A) UV-Vis absorption spectra. Concentration: 6.25 μmol $L^{-1}$. (B) Intrinsic fluorescence emission spectra. Concentration: 25 μmol $L^{-1}$. (C) Singlet oxygen productivity (the absorbance decay at 372 nm with different irradiation time) of MB and $C_{12}$-MB detected by 9,10-diphenylanthracene oxidation. (D) Singlet oxygen productivity kinetics fitted with a pseudo-first order model.

Singlet oxygen productivity and kinetics have been disclosed with DPA oxidation according to Steinbeck's methods,[22] and the absorption decay at 372 nm with different irradiation time was used to calculate singlet oxygen productivity as shown in Fig. 3(C). In order to demonstrate singlet oxygen kinetics, the curves in Fig. 3(C) were fitted with a pseudo-first order model and were shown in Fig. 3(D). The reaction rate constant of singlet oxygen generation could be acquired from the slope of first order kinetic equation. Then, the rate constant of singlet oxygen of $C_{12}$-MB and MB is $-0.0033\ s^{-1}$ and $-0.03081\ s^{-1}$, respectively. The rate constant of singlet oxygen production by MB is almost with 10-fold to that by $C_{12}$-MB. The results demonstrated that the rate of singlet oxygen by $C_{12}$-MB is seriously inhibited by the existence of long hydrocarbon chain. Due to amphiphilicity, $C_{12}$-MB could form aggregates which can reduce their ability to absorb light and decrease the lifetime and quantum yield of the excited triplet state, which have been reported in Plaetzer's research.[32] In addition, electronic features of $C_{12}$-MB photosensitizers may also play a role. According to Matshitse's[33] and Shi's[34] results, the extra positive charges of the quaternary ammonium salt improved triplet quantum yields and shortened fluorescence lifetime, which could result in short intersystem crossing lifetime and lower $^1O_2$ production.

### 3.4 *In vitro* antibacterial photodynamic efficiency

Two kinds of typical pathogenic bacteria, *P. aeruginosa* and *S. aureus*, were used to evaluate the antibacterial photodynamic activity of MB and $C_{12}$-MB, and the corresponding results have been shown in Fig. 4. Fig. 4(A) and (B) are the digital images of colonies present in the plate. PBS and antibiotic groups indicated the negative and positive controls, respectively. Obviously, no colony could be found on the $C_{12}$-MB plate with light irradiation whatever *P. aeruginosa* and *S. aureus*. However, there were many colonies on the PBS and antibiotic plates, which showed the superior antibacterial photodynamic activity of $C_{12}$-MB with light irradiation. $\log_{10}$ CFU reduction has been calculated according to the results of Fig. 4(A) and (B) and illustrated by histogram in Fig. 4(C). As previously found in Fig. 4(A) and (B), it is obvious that $C_{12}$-MB with light caused the greatest $\log_{10}$ CFU reduction and achieved 4.27 and 4.8 for *P. aeruginosa* and *S. aureus*, respectively. In comparison, the $\log_{10}$ CFU reductions of $C_{12}$-MB without light are 2.3 and 0.9, which implied that light was the key of enhancing antibacterial activity of $C_{12}$-MB. On the other hand, $C_{12}$-MB without light showed moderate antibacterial activity compared to negative control, which could originate from the quaternary ammonium structure of $C_{12}$-MB. Many quaternary ammonium surfactants showed antibacterial

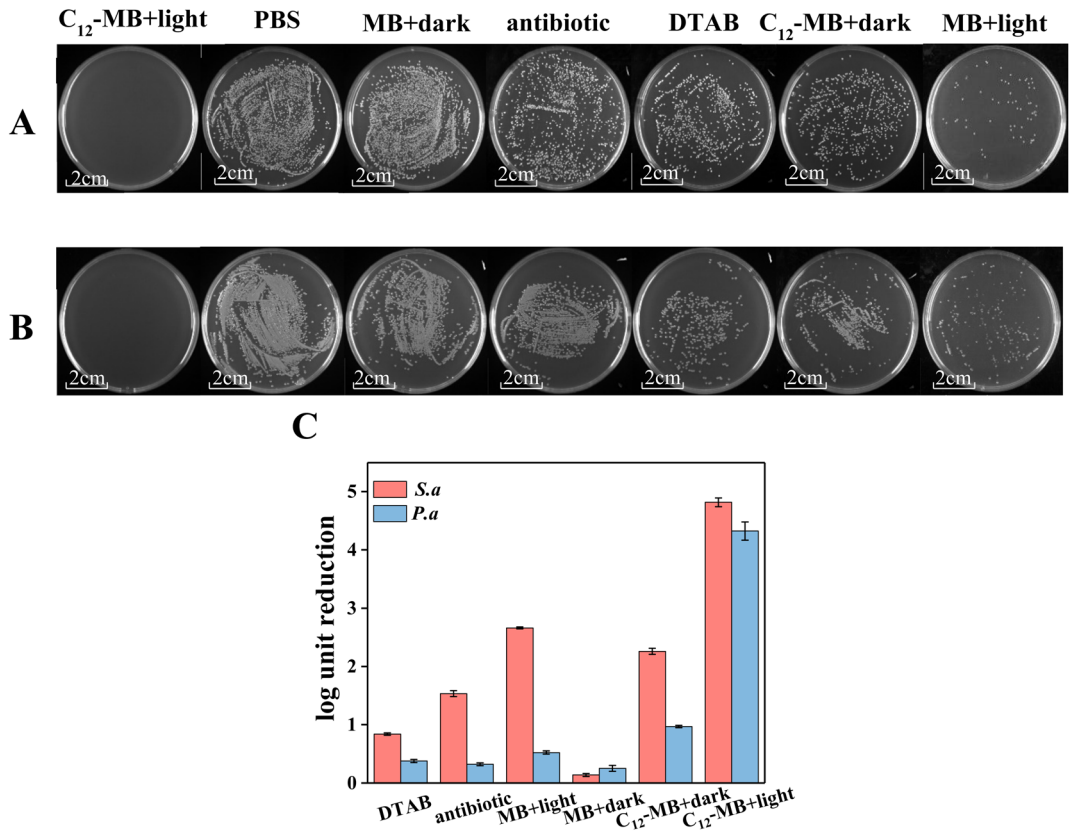


Fig. 4 *In vitro* antibacterial photodynamic activity. Photographs of plate samples of Gram-negative *P. aeruginosa* (A) and Gram-positive *S. aureus* (B) treated with APDT. For APDT, bacteria were incubated with $C_{12}$-MB or MB (200 μM, equivalent MB) and exposed to 660 nm LED light at 30 mW $cm^{-2}$ for 20 min. Antibiotics vancomycin and cefixime (100 mg $L^{-1}$) were used for *S. aureus* and *P. aeruginosa*, respectively, as control. (C) APDT activity was quantitated by counting colony forming units per milliliter (CFU $mL^{-1}$) and reduction in the log unit compared to the DTAB group and antibiotics group.

activity and were the most commonly material in disinfectants.[35] Comparing with the typical quaternary surfactant DTAB, $C_{12}$-MB without light showed higher antibacterial activity, which indicated that di-cationic structure or phenothiazine structure could contribute to higher antibacterial performance.

The strong antibacterial photodynamic activity of $C_{12}$-MB could originate from amphiphilic di-cationic photosensitizers with strong surface activity. Juliana *et al.* studied the effect of surfactants structure on APDT.[19] Further, the cationic surfactants showed the best effect on APDT because of its positive charge. In the other paper, Ariane *et al.* have prepared six different methylene blue derivatives successfully and concluded that additional positive charges could promote antibacterial activity on APDT.[36] In our study, $C_{12}$-MB is a di-cationic surfactant with the structure of quaternary ammonium formed by MB and long hydrocarbon chain. Hydrophilic phenothiazine structure provides two positive charges, which could increase the combination of bacteria and photosensitizers. At the same time, the long hydrocarbon chain could insert the lipid bilayers of the cells and improve the binding force. The similar mechanism of action has been reported in some literature.[37,38] The hydrophobic palmitic acid and the hydrophilic RRRR peptide with positively charges are the key for nanoparticles to targeted absorbed by cell membrane.[37,38] In conclusion, the synergetic effect of the phenothiazine structure with two positive charges and long hydrocarbon chain would promote $C_{12}$-MB photosensitizers adsorption on the cell membrane to improve antibacterial photodynamic activity.

To explore the influence of APDT on the bacterial envelop integrity, scanning electronic microscopy was used to record the cells morphology changes, and the corresponding results were shown in Fig. 5. Two kinds of bacteria remained integrity after antibacterial photodynamic treatments with either MB or $C_{12}$-MB, which indicated that antibacterial photodynamic treatment couldn't lead to bacterial envelop damage. According to some previous studies,[39,40] MB couldn't induce obvious damage to cell membrane. Therefore, the possible mechanism of $C_{12}$-MB is inactivating bacteria based on molecular scale interaction between singlet oxygen and important biological objects, such as lipid bilayers, proteins or nucleic acid. The loss of biological function induced by cytotoxic singlet oxygen oxidation cannot be observed by scanning electron microscopy.

### 3.5 Photosensitizers accumulation over bacterial cells

High accumulation of photosensitizers is a prerequisite for efficient antibacterial photodynamic therapy. When the bacterial suspensions ($10^8$ CFU $ml^{-1}$) were incubated with photosensitizers (400 mM) for 30 min at 25 °C, the adsorption amounts of methylene blue were 1064 and 1315 nmol/$10^8$ cells over *P. aeruginosa* and *S. aureus*. In comparison, the adsorption amounts of $C_{12}$-MB were 429 and 731 nmol/$10^8$ cells over *P. aeruginosa* and *S. aureus*. When these bacterial cells with adsorbed photosensitizers were washed with PBS solution repeatedly, the residual quantity of photosensitizers were determined and plotted in Fig. 6(A). The final retention ratio of $C_{12}$-MB on *P. aeruginosa* and *S. aureus* is 65.57% and 38.61%, respectively. By comparison, MB retention is only 42.06% and 27.72%. It is obvious that $C_{12}$-MB retention is larger than MB, which could be ascribed to the hydrocarbon tail of $C_{12}$-MB insertion into cell membrane. From the fluorescence images as shown in Fig. 6(B) and (C), two kinds of bacterial strains with adsorbed $C_{12}$-MB showed bright red fluorescence, which indicated that more photo-active photosensitizers had been adsorbed over bacterial surfaces. On the contrary, the bacterial cells with adsorbed MB showed much weaker fluorescence. The photosensitizers over bacterial cells have been quantified by fluorescence spectra according to the standard curves, and the corresponding results were shown in Fig. 6(D). The accumulation of $C_{12}$-MB over *P. aeruginosa* is 543.3 nmol/$10^8$ cells, higher than the adsorbed MB amount of 193 nmol/$10^8$ cells. On the other hand, the adsorption amounts of $C_{12}$-MB and MB on *S. aureus* are 140 and 732 nmol/$10^8$ cells, which was opposite to that on *P. aeruginosa*.

As a kind of planar aromatic molecules, methylene blue is prone to aggregate and form multi-layer adsorption through weak physical forces. Therefore, higher adsorption amounts of MB over *P. aeruginosa* and *S. aureus* were observed. However, these MB molecules are easily desorbed during washing

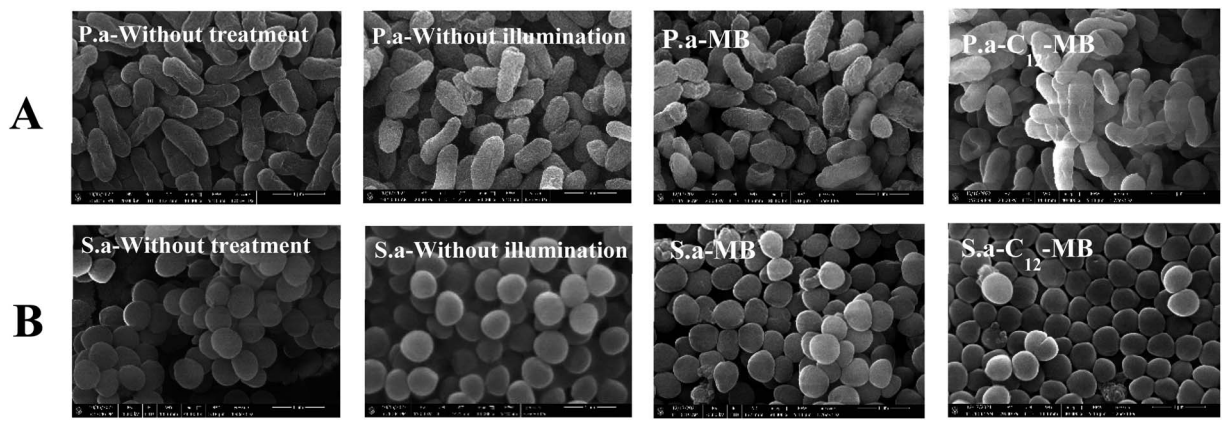


Fig. 5 Bacterial morphology observation by scanning electronic microscopy after photodynamic treatment by MB and $C_{12}$-MB. Images of *P. aeruginosa* (A) and *S. aureus* (B) treated by APDT of without treatment, without illumination, MB and $C_{12}$-MB.

 

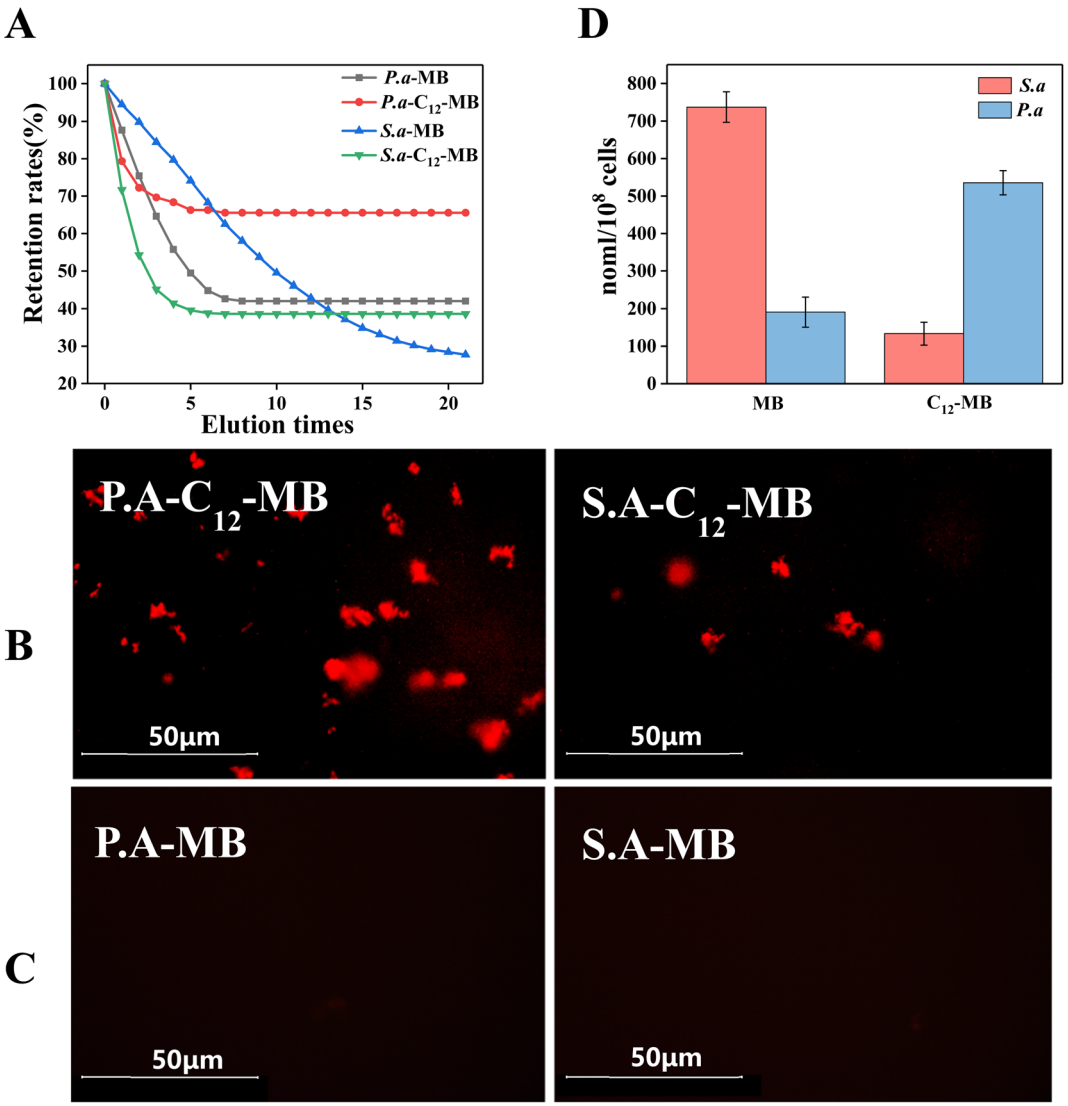


Fig. 6 The cellular accumulations of MB and $C_{12}$-MB by *S. aureus* and *P. aeruginosa*. (A) The photosensitizers retention ratio after elution repeatedly. (B) Fluorescence microscope photographs of *S. aureus* incubated with $C_{12}$-MB. (C) Fluorescence microscope photographs of *P. aeruginosa* incubated with MB. (D) The cellular accumulations of MB or $C_{12}$-MB by *S. aureus* and *P. aeruginosa* quantified by fluorescence spectra methods.

process. In contrast, $C_{12}$-MB could be adsorbed through hydrophobic interaction between alkyl chain and lipid membrane. Due to the spatial orientation of adsorbed $C_{12}$-MB molecules, it is difficult to form planar packing, which could contribute lower adsorption amount over bacterial cells.

On the other way, the adsorption amount of $C_{12}$-MB on *P. aeruginosa* is also greater than that on *S. aureus*, which could attribute to differences in the cell wall structure between Gram-negative and Gram-positive bacteria. Unlike Gram-positive bacteria, the cell wall of Gram-negative bacteria lacks the structure of thick peptidoglycan.[41] Instead, Gram-negative bacteria owns the lipopolysaccharide component of the outer membrane, which are rich in negatively charged lipid A.[37] Lipopolysaccharide with negative charges and di-cationic $C_{12}$-MB attract to each other, which could contribute to the strong binding with Gram-negative bacteria than MB.

### 3.6 Photosensitizers aggregation states over bacterial cells surface

It is well known that the methylene blue aggregation affects its photodynamic efficiency. The dimer-form of MB could produce reactive oxygen species (ROS) through type I sensitization mechanism, and practically impare $^1O_2$ generation through type II sensitization process.[42] In fact, compared with other ROS, singlet oxygen has stronger oxidation capacity and better photodynamic efficiency. Therefore, in the delivery system of methylene blue, the content of monomer state is improved by various methods, such as reducing the concentration, using surfactants, using liposomes and so on.[43–45] However, little attention is paid to the fact that whether methylene blue can maintain the monomer state with high photodynamic efficiency after adsorption on the cell surface. In order to compare the

possible mechanism of APDT of amphiphilic photosensitizer $C_{12}$-MB, we studied the photosensitizer aggregation on the surface of bacterial cells by spectroscopy, and the results are shown in Fig. 7. Compared the UV-Vis spectra of MB and $C_{12}$-MB solution in Fig. 3(A), the absorption pattern of the photosensitizer adsorbed on the cell surface changed significantly, and multiple absorption peaks appeared as seen in Fig. 7(A). According to Patil' report, the absorption peak at 660 nm could be attributed to the monomer of methylene blue, while the second peak varies from about 605 nm (related to the dimer) to about 585 nm (which can be probably attributed to the prevailing tetramer or even higher aggregates of the dye).[46,47] The ratio of monomer and multi-mer was calculated based on absorption peaks area at 660 nm and lower than 660 nm, and the quantitative histogram has been shown in Fig. 7(C). Due to the planar structure of phenothiazine ring, its adsorption aggregation is easy to produce H aggregation. The monomer percentage of MB adsorbed on the surface of *P. aeruginosa* is significantly reduced, while the content of dimer and other multi-mer is significantly increased. The corresponding fluorescence intensity in Fig. 7(B) is also significantly reduced, indicating that methylene blue produces significant H aggregation on the surface of *P. aeruginosa* cells, resulting in the decrease of fluorescence intensity. Different from a large number of trimers or multimers produced by MB, the absorption peaks of $C_{12}$-MB on the bacterial cell surface are located at 660 nm and 615 nm, which corresponds to monomers and dimers respectively.[40] These results demonstrated that the existence state of amphiphilic $C_{12}$-MB on the cell surface is monomers and dimers, and the monomer content is obviously higher than that of MB. Moreover, as seen from Fig. 7(C), the monomer contents of $C_{12}$-MB adsorbed on *P. aeruginosa* and *S. aureus* cells are 73% and 70%, respectively, which are higher than those of 25% and 49% MB monomer contents. Meanwhile, the fluorescence intensity in Fig. 7(B) is also significantly stronger than MB, which confirms that the monomer state is the active state of photodynamic therapy. Totally, after $C_{12}$-MB is adsorbed on the surface of bacterial cells, it can maintain a high percent of monomer state, which will directly contribute to the high APDT efficiency.

Based on the above results, we proposed a possible mechanism of amphiphilic $C_{12}$-MB enhancing APDT efficiency as shown in Fig. 8. The specific peptidoglycan or lipopolysaccharide on the surface of bacterial cells endows the cell surface with negative charge. Therefore, cationic MB can be adsorbed on the cell surface through electrostatic adsorption. Once MB is

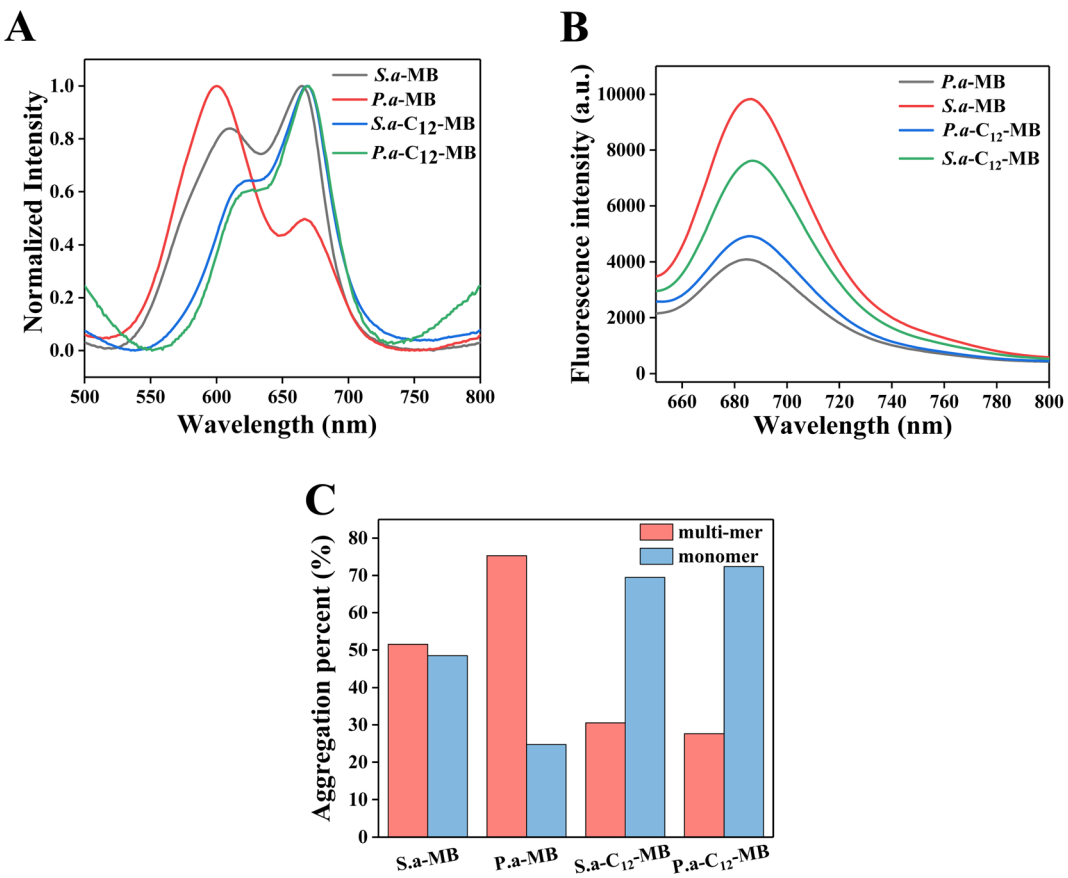


Fig. 7 The spectroscopic characterization of adsorbed MB and $C_{12}$-MB over *S. aureus* and *P. aeruginosa*. (A) UV-Vis absorption spectra with normalized intensity. (B) Fluorescence emission spectra. (C) The quantitative histogram of monomer and multi-mer(dimer, trimer, tetramer and other higher aggregation) based on absorption peaks area ratio at 660 nm and other lower than 660 nm(such as 615 nm, 600 nm, 580 nm, 560 nm).

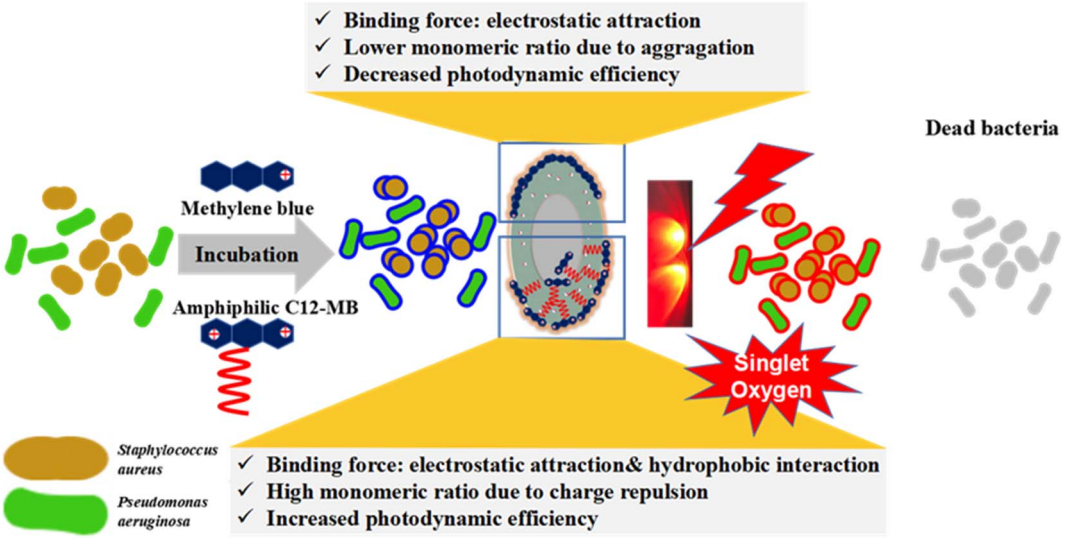


Fig. 8 A possible hypothesis of higher APDT efficiency with amphiphilic $C_{12}$-MB.

neutralized by the negative charge on the cell surface, it will no longer have charge. Therefore, it is easy to accumulate with other MB molecules, resulting in dimers, trimers and multimers. The quantitative results demonstrate that the photoactive MB monomer accounts for only 25% and 49% over *P. aeruginosa* and *S. aureus*, which could induce lower APDT efficiency. In contrast, the as-synthesized amphiphilic di-cationic photosensitizer $C_{12}$-MB contains both hydrophobic chain and two quaternary ammonium structures. Therefore, when $C_{12}$-MB interacts with the cell surface, it may interact with plasma membrane through hydrophobic interaction and electrostatic interaction. Under the cooperation of two factors, $C_{12}$-MB binds firmly to the surface of bacterial cells and is difficult to elute, as shown in Fig. 6. On the other hand, after part of the positive charges of $C_{12}$-MB is neutralized by the cell surface, the remaining positive charge repulsion can reduce photosensitizer aggregation. Moreover, since the amphiphilic $C_{12}$-MB will decrease the planar accumulation possibility on the cell surface after the hydrophobic chain is inserted into the cell plasma membrane, $C_{12}$-MB molecules could exist in the prevailing monomers form on the cell surface, such as 73% and 70% over *P. aeruginosa* and *S. aureus*, which could contribute to the higher APDT efficiency.

## 4 Conclusion

In conclusion, we have successfully synthesized a kind of amphiphilic di-cationic photosensitizers $C_{12}$-MB for antibacterial photodynamic therapy. $C_{12}$-MB under 660 nm illumination could inactivate *P. aeruginosa* and *S. aureus with* the CFU 4.8 $\log_{10}$ and 4.27 $\log_{10}$, higher than $\log_{10}$ 2.3 and $\log_{10}$ 0.9 of MB. Amphiphilic photosensitizers $C_{12}$-MB could remain photoactive monomer content of 73% and 70% over *P. aeruginosa* and *S. aureus* surfaces, higher than those of MB 25% and 49%, respectively. The spectroscopic characterization of adsorbed MB and $C_{12}$-MB over bacterial cells demonstrated that the higher antibacterial photodynamic therapy could originate from higher $C_{12}$-MB photosensitizers monomer percentage. The amphiphilic and di-cationic structures could contribute to the high accumulation and low aggregation of photosensitizers over those biological targets, which could produce outstanding antibacterial photodynamic efficiency.

## Author contributions

Hao Zhang: Data curation, Methodology, Investigation. Lixian Xu: Clinical research idea and data curation, Writing – review & editing. Xiaoxiao Gu: Conceptualization, Methodology, Review. Shuang Li: Microbacterial data curation, Funding acquisition. Dinghua Yu: Supervision, Data curation, Funding acquisition, Project administration.

## Conflicts of interest

The authors declare that they have no known competing financial interests or personal relationships that could have appeared to influence the work reported in this paper.

## Acknowledgements

This work was supported by the National Key Research and Development Plan (No. 2021YFC2103800), Six Talent Peaks Project in Jiangsu Province (No. 2018-GDZB-196) and the Jiangsu Synergetic Innovation Center for Advanced Bio-Manufacture.

## References

1 A. Grzybowski and M. Turczynowska, *Asia-Pac. J. Ophthalmol.*, 2018, **7**, 72–75.
2 S. Reardon, *Nature*, 2014, **10**, 15135.

3 F. Cieplik, D. Deng, W. Crielaard, W. Buchalla, E. Hellwig, A. Al-Ahmad and T. Maisch, *Crit. Rev. Microbiol.*, 2018, **44**, 571–589.
4 X. Wang, Z. Yuan, A. Tao, P. Wang, W. Xie, S. Yang, J. Huang and N. Wen, *Biomaterials*, 2022, **281**, 121377.
5 X. Wei, L. Liu, X. Guo, Y. Wang, J. Zhao and S. Zhou, *ACS Appl. Mater. Interfaces*, 2018, **10**, 17672–17684.
6 P. Rundle, *Biomedicines*, 2017, **5**, 69.
7 X. Ma, Q. Qu and Y. Zhao, *ACS Appl. Mater. Interfaces*, 2015, **7**, 10671–10676.
8 T. Kimura, S. Takatsuki, S. Miyoshi, K. Fukumoto, A. Ito, M. Takahashi, E. Ogawa, S. Motohashi, T. Arai and K. Fukuda, *Eur. Heart J.*, 2013, **34**, 345.
9 C. C. Jayme, I. R. Calori and A. C. Tedesco, *Spectrochim. Acta, Part A*, 2016, **153**, 178–183.
10 G. A. da Collina, F. Freire, T. Santos, N. G. Sobrinho, S. Aquino, R. A. Prates, D. F. T. da Silva, A. C. R. Tempestini Horliana and C. Pavani, *Photochem. Photobiol. Sci.*, 2018, **17**, 1355–1364.
11 X. Cheng, J. Gao, Y. Ding, Y. Lu, Q. Wei, D. Cui, J. Fan, X. Li, E. Zhu, Y. Lu, Q. Wu, L. Li and W. Huang, *Adv. Sci.*, 2021, **8**, 2100876.
12 G. Boccalini, L. Conti, C. Montis, D. Bani, A. Bencini, D. Berti, C. Giorgi, A. Mengoni and B. Valtancoli, *J. Mat. Chem. B*, 2017, **5**(15), 2788–2797.
13 J. Wang, Y. Zhong, X. Wang, W. Yang, F. Bai, B. Zhang, L. Alarid, K. Bian and H. Fan, *Nano Lett.*, 2017, **17**, 6916–6921.
14 M. Usacheva, S. K. Swaminathan, A. R. Kirtane and J. Panyam, *Mol. Pharm.*, 2014, **11**, 3186–3195.
15 G. Jaber, R. Dariush, A. Shahin, T. Alireza and B. Abbas, *Laser Ther.*, 2018, **27**, 293–302.
16 E. Baigorria, J. E. Durantini, M. A. Di Palma, N. S. Gsponer, M. E. Milanesio and E. N. Durantini, *Photochem. Photobiol. Sci.*, 2021, **20**, 939–953.
17 L. Conti, A. Mengoni, G. E. Giacomazzo, L. Mari, M. Perfetti, C. Fagorzi, L. Sorace, B. Valtancoli and C. Giorgi, *J. Inorg. Biochem.*, 2021, **220**, 111467.
18 V. H. Panhoca, F. L. E. Florez, T. Q. Correa, F. R. Paolillo, C. W. O. de Souza and V. S. Bagnato, *Photomed. Laser Surg.*, 2016, **34**, 411–417.
19 J. P. Lyon, R. R. Rezende, M. P. Rabelo, C. J. de Lima and L. M. Moreira, *Mycopathologia*, 2013, **175**, 159–164.
20 K. K. Karukstis, D. A. Savin, C. T. Loftus and N. D. D'Angelo, *J. Colloid Interface Sci.*, 1998, **203**, 157–163.
21 T. Zhou, M. Ao, G. Xu, T. Liu and J. Zhang, *J. Colloid Interface Sci.*, 2013, **389**, 175–181.
22 M. J. Steinbeck, A. U. Khan and M. J. Karnovsky, *J. Biol. Chem.*, 1992, **267**, 13425–13433.
23 J. Zhao, L. Xu, H. Zhang, Y. Zhuo, Y. Weng, S. Li and D. Yu, *Colloids Surf., B*, 2021, **207**, 111974.
24 G. Sych, R. Pashazadeh, Y. Danyliv, O. Bezvikonnyi, D. Volyniuk, A. Lazauskas and J. V. Grazulevicius, *Chem.–Eur. J.*, 2021, **27**, 2826–2836.
25 K. K. Nichols, B. M. Ham, J. J. Nichols, C. Ziegler and K. B. Green-Church, *Invest. Ophthalmol. Vis. Sci.*, 2007, **48**(1), 34–39.
26 Q. Zhang, M. H. Chen, L. J. Zhong, Q. Ye, S. S. Jiang and Z. J. Huang, *Molecules*, 2018, **23**(8), 2086.
27 R. Zana, *Adv. Colloid Interface Sci.*, 2002, **97**, 205–253.
28 T. Kato, T. Nakamura, M. Yamashita, M. Kawaguchi, T. Kato and T. Itoh, *J. Surfactants Deterg.*, 2003, **6**, 331–337.
29 M. Miyake, K. Yamada and N. Oyama, *Langmuir*, 2008, **24**, 8527–8532.
30 A. Khadieva, O. Mostovaya, P. Padnya, V. Kalinin, D. Grishaev, D. Tumakov and I. Stoikov, *Int. J. Mol. Sci.*, 2021, **22**, 5847.
31 J. Cao, C. Meng and H. Zhao, *Color. Technol.*, 2017, **134**, 111–116.
32 K. Plaetzer, B. Krammer, J. Berlanda, F. Berr and T. Kiesslich, *Laser Med. Sci.*, 2009, **24**, 259–268.
33 R. Matshitse, N. Nwaji, M. Managa, Z. L. Chen and T. Nyokong, *Photodiagnosis Photodyn. Ther.*, 2022, **37**, 102705.
34 X. J. Shi, S. H. P. Sung, J. H. C. Chau, Y. Li, Z. Y. Liu, R. T. K. Kwok, J. K. Liu, P. H. Xiao, J. J. Zhang, B. Liu, J. W. Y. Lam and B. Z. Tang, *Small Methods*, 2020, **4**(7), 2000046.
35 C. P. Gerba, *Appl. Environ. Microbiol.*, 2015, **81**, 464–469.
36 A. Felgentrager, T. Maisch, D. Dobler and A. Spath, *BioMed Res. Int.*, 2013, **2013**, 482167.
37 W. Ma, S. N. Sha, P. L. Chen, M. Yu, J. J. Chen, C. B. Huang, B. Yu, Y. Liu, L. H. Liu and Z. Q. Yu, *Adv. Healthcare Mater.*, 2020, **9**, 1901100.
38 L. H. Liu, W. X. Qiu, Y. H. Zhang, B. Li, C. Zhang, F. Gao, L. Zhang and X. Z. Zhang, *Funct. Mater.*, 2017, **27**, 1700220.
39 J. H. Yin, Q. Meng, D. Cheng, J. Fu, Q. X. Luo, Y. Q. Liu and Z. L. Yu, *Appl. Microbiol. Biotechnol.*, 2020, **104**, 3771–3780.
40 J. Rolim, M. A. S. de-Melo, S. F. Guedes, F. B. Albuquerque, J. R. de Souza, N. A. P. Nogueira, I. C. J. Zanin and L. K. A. Rodrigues, *J. Photochem. Photobiol. B*, 2012, **106**, 40–46.
41 V. R. F. Matias and T. J. Beveridge, *Mol. Microbiol.*, 2005, **56**, 240–251.
42 H. C. Junqueira, D. Severino, L. G. Dias, M. S. Gugliotti and M. S. Baptista, *Phys. Chem. Chem. Phys.*, 2002, **4**(11), 2320–2328.
43 J. Yu, C. Hsu, C. Huang and P. Chang, *ACS Appl. Mater. Interfaces*, 2015, **7**, 432–441.
44 B. Sharma, G. Kaur, G. R. Chaudhary, S. L. Gawali and P. A. Hassan, *Biomater. Sci.*, 2020, **8**, 2905–2920.
45 Y. Y. Li, J. M. Xiong, Y. Hu, W. J. Miao and H. He, *J. Leather Sci. Eng.*, 2022, **4**, 31.
46 K. Patil, R. Pawar and P. Talap, *Phys. Chem. Chem. Phys.*, 2000, **2**, 4313–4317.
47 E. Touitou and P. Fisher, *J. Pharm. Sci.*, 1986, **75**, 384–386.